NASA-CR-202437

NASA GRANT NAG-1-1610

THE PHYSICS OF TURBULENCE IN THE BOUNDARY LAYER

Final Report submitted to the
NASA Langley Research Center
Hampton, VA 23665-5225

Funding Dates: April 25, 1994 to October 24, 1995

University Investigators
Stephen Kline
Department of Mechanical Engineering
Stanford University, Stanford, CA 94305
and
Brian Cantwell
Department of Aeronautics and Astronautics
Stanford University, Stanford, CA 94305

NASA-Langley Point of Contact
Stephen Robinson
Mail Stop163, NASA Langley Research Center
Hampton, VA 23665-5225

October 1996

1. SUMMARY

The geometry of the velocity field in a numerically simulated incompressible turbulent boundary layer over a flat plate at Reθ=670 has been studied using the invariants of the velocity gradient tensor. These invariants are computed at every grid point in the flow and used to form the discriminant. Of primary interest are those regions in the flow where the discriminant is positive; regions where, according to the characteristic equation, the eigenvalues of the velocity gradient tensor are complex. An observer moving with a frame of reference which is attached to a fluid particle lying within such a region would see a local flow pattern of the type stable-focus-stretching or unstable-focus-compressing. When the flow is visualized this way, continuous, connected, large-scale structures are revealed that extend from the point just below the buffer layer out to the beginning of the wake region.. These structures are aligned with the mean shear close to the wall and arch in the cross-stream direction away from the wall. In some cases the structures observed are very similar to to the hairpin eddy vision of boundary layer structure proposed by Theodorsen. That the structure of the flow is revealed more effectively by the discriminant rather than by the vorticity is important and adds support to recent observations of the discriminant in a channel flow simulation. Further details can be found in the attached paper by Chacin, Cantwell and Kline. Of particular importance is the fact that the procedure does not require the use of an arbitrary threshold in the discriminant. Further analysis using computer flow visualization shows a high degree of spatial correlation between regions of positive discriminant, extreme negative pressure fluctuations and large instantaneous values of Reynolds shear stress.

Further details of the work carried out under this grant can be found in the paper by Chacin, Cantwell and Kline a copy of which is attached to this report.

2. PUBLICATIONS

Chacin, J., B. J. Cantwell, S. J. Kline 1996 Study of turbulent boundary layer structure using the invariants of the velocity gradient tensor. *Journal of Experimental Thermal and Fluid Science* (to appear).

Submitted for publication to the *Journal of Experimental Thermal and Fluid Science*

Study of turbulent boundary layer structure using the invariants of the velocity gradient tensor

Juan M. Chacín
Department of Mechanical Engineering
Stanford University
Stanford, CA, 94305
e-mail: *chacin@stokes.stanford.edu*

Brian J. Cantwell
Department of Aeronautics and Astronautics
Durand Building, Room 271, MC: 4035
Stanford University
Stanford, CA, 94305
Phone: (415) 723-4825
FAX: (415) 725-3377
e-mail: *cantwell@leland.stanford.edu*
Please address all correspondence to this author

Stephen J. Kline
Department of Mechanical Engineering
Stanford University
Stanford, CA, 94305
e-mail: *kline@stokes.stanford.edu*

Study of turbulent boundary layer structure using the invariants of the velocity gradient tensor

Juan M. Chacín[1], Brian J. Cantwell[2]
and Stephen J. Kline[1]

[1] Department of Mechanical Engineering, Stanford University, Stanford, CA, 94305
[2] Department of Aeronautics and Astronautics, Stanford University, Stanford, CA, 94305

June 24, 1996

Abstract

The geometry of the velocity field in a numerically simulated incompressible turbulent boundary layer over a flat plate at $Re_\theta = 670$ is studied using the invariants of the velocity gradient tensor (P, Q and R). These invariants are computed at every grid point in the flow and used to form the discriminant ($D = 27R^2/4 + Q^3$). Of primary interest are those regions in the flow where the discriminant is positive; regions where, according to the characteristic equation, the eigenvalues of the velocity gradient tensor are complex. An observer moving with a frame of reference which is attached to a fluid particle lying within such a region would see a local flow pattern of the type stable-focus-stretching or unstable-focus-compressing. When the flow is visualized in this way, continuous, connected, large scale structures are revealed that extend from the just below the buffer layer ($y^+ \approx 1.0$) out to the beginning of the wake region. These structures are aligned with the mean shear close to the wall and arch in the cross-stream direction away from the wall. In some cases the structures observed are very similar to the hairpin eddy vision of boundary layer structure proposed by Theodorsen [1]. Recently this conceptual picture has been used by Perry *et. al.* [2] to develop a successful model of the turbulent boundary layer based on an extension of the attached eddy hypothesis first proposed by Townsend [3]. That the structure of the flow is revealed more effectively by the discriminant rather than by the vorticity

is important and adds support to the recent analysis of channel flow structure by Blackburn *et. al.* [4]. Of particular importance (and also in contrast to the use of the vorticity) is the fact that the procedure does not require the use of an arbitrary threshold in the discriminant. Further analysis using computer flow visualization shows a high degree of spatial correlation between the regions of positive discriminant, extreme negative pressure fluctuations and large instantaneous values of Reynolds shear stress ($u'v'$).

Keywords: Turbulence structure, flow topology, topological invariants, discriminant.

1 Introduction

Recent years have seen an explosion in the amount, and type, of data available on turbulent flows. In addition to better and more accurate experimental measuring techniques, the advent of direct numerical simulations has created the possibility of "virtual" wind tunnels; ones with large amounts of primitive flow field information that can be accessed and analyzed repeatedly, almost on demand. However, before such analysis can be done, it is important to find a way to recast the vast information that is available in a form that will reveal the most dynamically significant aspects of the flow. In this work, phase-space methods and some basic concepts of vector field topology are used to accomplish this.

This method of studying fluid flows has been used in a variety of ways to study the geometry of flow patterns particularly near no-slip boundaries and in areas of flow separation and reattachment (see for example Taylor [5], Oswatitsch [6] or Perry *et. al.* [7]). Chong *et. al.* [8] considered a moving coordinate transformation in which the frame of reference remains attached to a given particle in the flow. They used the velocity gradient tensor invariants to map out a local description of all the various streamline patterns which can occur in a three-dimensional, linear flow (a flow with non-degenerate lowest order term in a Taylor series expansion). The result is a precisely defined, frame independent way of describing structural features of the flow. As will be shown, the method also removes the need for a threshold in the variable used to visualize the flow.

Many of the recent applications of this technique to turbulent flows have been to the study of the small scale, dissipating motions in the flow (see for example Chen *et. al.* [9], Soria and Cantwell [10], Soria *et. al.* [11],

and Boratav and Pelz [12]). In those cases, the objective was to look at the universality of fine-scale motions expressed in terms of joint PDF's of the velocity gradient tensor invariants. The ultimate goal of this work is to eventually incorporate this knowledge into predictive schemes for the dissipation of turbulent kinetic energy. Such information could be of significant importance, not only for conventional turbulence modeling applications, but also for the potential development of better sub-grid scales models for Large Eddy Simulations.

The first application of this approach to the study of the intermediate scale, coherent motions in a wall bounded flow is the recent work by Blackburn *et. al.* [4] who analyzed one time realization of a channel flow computed at a Reynolds number of 7860, based on the half-width of the channel (Kim *et. al.* [13]). In that study, the authors used the discriminant to identify coherent structures which extended from a region very close to the wall all the way out to nearly the center of the channel.

In the present work, this method is applied to a turbulent velocity field obtained from the direct numerical simulation of a flat plate turbulent boundary layer carried out by Spalart [14]. The results agree with previous results regarding the topology of the small-scale motions but, by using computer-based flow visualization tools, it is possible to produce a interesting view of the larger scales structures in the flow and their spatial association with other turbulence statistical events such as Reynolds stresses and pressure fluctuations.

2 Methodology

Following Perry and Chong [15] and Chong *et. al.* [8], the geometry of the instantaneous streamlines in the neighborhood of any point in the flow, as seen by an observer moving with the local speed of the fluid, can be classified according to the nature of the eigenvalues, and associated eigenvectors, of the velocity gradient tensor ($\mathbf{A}_{ij} = \partial U_i/\partial x_j$) at that point. Such eigenvalues are the roots of the characteristic equation of $\mathbf{A}_{ij}$, which is given by

$$\lambda^3 + P\lambda^2 + Q\lambda + R = 0 \tag{1}$$

where P, Q and R are the tensor invariants. These invariants are

$$P = -tr\,[\mathbf{A}] \tag{2}$$

$$Q = \frac{1}{2}\left\{[tr\,(\mathbf{A})]^2 - tr\left(\mathbf{A}^2\right)\right\} \quad (3)$$

$$R = -det\,(\mathbf{A}) \quad (4)$$

where tr and det indicate the trace and the determinant of the tensor respectively. For the flow to be considered here, the first invariant (P) is identically zero because of the incompressibility condition. Hence, Eq. 1 reduces to

$$\lambda^3 + Q\lambda + R = 0 \quad (5)$$

The nature of the roots of this equation is determined by the values of the two remaining invariants Q and R. In particular, it can be shown that the line that defines the boundary (in the $Q - R$ plane) between the region where all the roots are real and the region where two roots are complex and one real is given by (see Chong *et. al.* [8] for the full details).

$$\frac{27}{4}R^2 + Q^3 = 0 \quad (6)$$

The discriminant of $\mathbf{A}_{ij}$ is

$$D = \frac{27}{4}R^2 + Q^3 \quad (7)$$

and it identifies the most basic topological information contained in the invariants Q and R. Specifically, for the points in the flow where $D > 0$, Eq. 5 admits two complex and one real solutions. These points are called foci. If $D < 0$ all the solutions are real and the point is called a node-saddle-saddle according to the terminology adopted by Chong *et. al.* [8].

Figure 1: Idealized streamline pattern around a focus critical point.

Figure 1 is an idealized sketch of the instantaneous streamlines in the neighborhood of a focus point ($D > 0$). The specific direction that a fluid particle would follow along those streamlines is determined by the sign of the third invariant of $\mathbf{A}_{ij}$, R, and by the incompressibility condition. If R is

positive, the focus is said to be unstable. In this case, the fluid moves away from the center in the plane of the spirals and, because of incompressibility, it moves towards the center along the axis (compression). If R is negative, the direction of motion is reversed. The fluid moves towards the center in the spiral plane and away from it along the axis (stretching). This is called a stable focus.

Figure 2: Idealized streamline pattern around a node-saddle-saddle critical point.

Figure 2 is a sketch of a node-saddle-saddle point ($D < 0$) and, again, the direction of motion along the streamlines will be determined by the sign of the third invariant and the requirement of mass conservation.

Using this technique, the two non-zero invariants of the velocity gradient tensor Q and R, and its discriminant D, can then be used to classify the topology of every point in a three dimensional flow field according to its position on the two dimensional $Q - R$ plane. This is summarized in Fig. 3

Figure 3: Summary of three dimensional incompressible topologies (from Soria *et. al.* [11]).

It is important to notice that $\mathbf{A}_{ij}$, and all its invariants, remain constant under a non-uniform translation. This means that, even though an observer translating (not rotating) at an arbitrary velocity may see see a streamline pattern different from than that shown on Figs. 1 and 2, the topological classification of such point will be the same, independently of the frame of reference.

3 Results

The topological classification method described in the previous section was used to study the velocity field obtained from the spectral direct numerical simulation of a turbulent boundary layer under zero pressure gradient done by P. R. Spalart (see Spalart [14]). All the results presented here are for a Reynolds number, based on momentum thickness (Re_θ), of 670.

The approach used is similar to that used by Chen *et. al.* [9], Soria *et. al.* [11] and Blackburn *et. al.* [4]. At every grid point in the simulation, all nine components of the velocity gradient tensor were computed using a spectral series expansion consistent with that used in the DNS calculation. From them, the invariants (Q and R) of $\mathbf{A}_{ij}$ were obtained using Eqs. 2 - 4 and used to classify the geometry of the local streamlines according to their position in the $Q - R$ plane. At every time realization of the simulation, all four types of three-dimensional topologies are present in the flow field but with different probabilities. Figure 4 shows a time-averaged, unnormalized, joint probability distribution for Q and R constructed from a total sample of more than 141 million data points gathered over 90 realizations. The axes of the plot are not normalized so the values are in physical units. Four contours of equal probability levels with logarithmic spacing are shown. The values associated with these contours (shown in the legend at the foot of the figure) correspond to the density of data points per unit area of the plot, per simulation time step.

Figure 4: Time-averaged, unnormalized joint probability density distributions for the second and third invariants of the velocity gradient tensor (Q and R). The dashed lines are lines of constant discriminant (Eq. 7). The values grow or decrease as indicated by the arrows.

The contours in Fig. 4 show a tendency for the data to gather in a tear-drop or elongated elliptical region centered at the origin whose main axis is inclined to the left of the Q axis. Also, most of the points are clustered near the origin of coordinates. The inner-most (darkest) contour

has a density of data points 1000 times bigger than the outer-most one and contains almost 95% of the data. This tendency has also been observed in time-developing compressible and incompressible mixing layers (see Soria *et. al.* [11] and Chen *et. al.* [9]) as well as in turbulent channel flow (see Blackburn *et. al.* [4]). In spite of this, it can also be seen that significant excursions are also possible. Most of these excursions occur in the upper-left quadrant (stable-focus-stretching) and the lower-right quadrant (unstable-node-saddle-saddle). The fluid motions associated with these events can be analyzed further by dividing the velocity gradient tensor into its symmetric and antisymmetric parts

$$\mathbf{A}_{ij} = \mathbf{S}_{ij} + \mathbf{W}_{ij} \tag{8}$$

where

$$\mathbf{S}_{ij} = \frac{1}{2}\left(\frac{\partial U_i}{\partial x_j} + \frac{\partial U_j}{\partial x_i}\right) \tag{9}$$

$$\mathbf{W}_{ij} = \frac{1}{2}\left(\frac{\partial U_i}{\partial x_j} - \frac{\partial U_j}{\partial x_i}\right) \tag{10}$$

Using these relations, it is a simple matter to show that the second invariant (Q) can be written as

$$Q = \frac{1}{2}\left(\mathbf{W}_{ij}\mathbf{W}_{ij} - \mathbf{S}_{ij}\mathbf{S}_{ij}\right) \tag{11}$$

The first term on the right hand side of Eq. 11 is proportional to the total enstrophy, the second one is proportional to the kinetic energy dissipation rate. Both of these terms are non-negative. Then, for the points lying away from the origin in the upper-left quadrant, where Q is large and positive, the rate of rotation dominates the strain rate. For those points in the lower-right quadrant, where Q is large and negative, the vorticity is low compared to the rate of strain, indicating that these are motions with high levels of dissipation. It can also be seen in Fig. 4 that in the lower-right quadrant, near the "tail", the distribution is skewed towards the negative discriminant side of the Q - R plane. This means that regions of high dissipation are preferentially of the kind unstable-node-saddle-saddle.

Invariant plots like that shown in Fig. 4 have been used predominantly for the study of the small, dissipating scales in turbulent flows since these are the motions with the largest gradients of velocity and, hence, the largest

values of Q and R. Blackburn *et. al.* [4] then extended the application of this methodology to the study of the larger, energy containing scales of the flow. For this, it would be advantageous to combine the information contained in the two invariants into a single scalar quantity that could then be used to study the flow structure in physical space. The scalar they chose was the discriminant of the velocity gradient tensor, D (Eq. 7). As shown in Fig. 3, the discriminant divides the Q - R plane into two main regions. The upper one, where $D > 0$, corresponds to points with focus topology (stable or unstable depending on the sign of R) while the lower region, $D < 0$, is that of node-saddle-saddle topology, again stable or unstable depending on R. Using flow visualization software, it is then possible to construct isosurfaces of discriminant in physical space and use this scalar to study the spatial structure of the flow field. This is the approach used here.

Figure 5: Top view of the computational volume. The blue contours are regions of positive discriminant (focus topology). The vertical extent of the domain is from $y^+ \approx 1$ to $y^+ \approx 138$. All the areas that are not colored have topology of the type node-saddle-saddle

Figure 5 shows a large section of one realization of the DNS computational domain as seen from directly above. The dimensions shown on the coordinate axes have been non-dimensionalized by wall units (u_τ and ν). Regions of positive discriminant (focus topology), both stable and unstable, are shown in blue and are visualized by plotting surfaces of constant discriminant value ($D \approx 0$). These regions reveal continuous, connected flow structures of large scale. Near the wall, the individual structures are elongated in the streamwise direction and they intertwine to form large streaks, some of them over 800 wall units long. Away from the wall, near the beginning and into the log layer, these regions of focus topology tilt upwards and then across the mean flow to form hairpin or horseshoe shaped structures. Several of these structures are visible in the flow field, for example around $x^+ \approx 1036, z^+ \approx 600$ or $x^+ \approx 400, z^+ \approx 100$.

A close up view of one such hairpin, the one located within the red out-

Figure 6: a) Close up view of a near-wall region of positive discriminant. b) Side view of the same region. The vertical extent of the domain is from $y^+ \approx 1$ to $y^+ \approx 83$.

line in Fig. 5, is shown in Figs. 6 a) and b). Two different view points are used in order to show the three-dimensionality of the structure. The dimensions of this sub-volume, normalized by wall units, are 265 in the streamwise direction, 194 in the spanwise direction and, in the wall-normal one, it extends from $y^+ \approx 1$ to $y^+ \approx 83$. The shape of this structure is conspicuously reminiscent of the horseshoe shaped vortices that are believed to be the central structure in wall-bounded turbulence (see for example Theodorsen [1], Head and Bandyopadhyay [16] and Robinson [17]). In Fig. 6, a single surface of constant value of the discriminant was sufficient to define the entire structure from just over the wall into the log layer. Furthermore, the threshold value of that isosurface is unambiguously set by the value of the discriminant that divides the regions of different topologies in the $Q - R$ plane. This value is $D = 0$ and it is the same for all incompressible flows.

The advantage of this feature is illustrated by Fig. 7. On this plot, the same sub-volume shown in Fig. 6 is studied using two different techniques. Figure 7 a) shows isocontours of enstrophy or total vorticity magnitude. By looking again at Fig. 4, it can be seen that, for the majority of points in the flow were the discriminant has a large, positive value, the second invariant Q also has a large, positive value. From Eq. 11, these are motions where the rotation rate is large compared to the total dissipation (*i.e.* vortex tubes). In Fig. 7 a), a horseshoe shaped vortex tube that corresponds to the structure in Fig. 6 is somewhat visible near the log layer. This correspondence is consistent with Theodorsen [1] who, by looking at a simplified version of the enstrophy transport equation concluded that, in order for turbulence to be created and maintained near a no-slip boundary, it was necessary for vortex lines to arrange themselves in the shape of a horseshoe that leaned away from the wall and in the direction of the imposed shear. It is however very difficult to find a single value for the isocontour of enstrophy that can be used to reveal the entire structure, particularly near the wall where the mean shear, and the mean vorticity, are both high. In fact, Fig. 7 a) would be difficult to interpret by itself without the help of Fig. 6.

Figure 7: Close up view of near-wall region. a) Isocontours of total vorticity magnitude. b) Isocontours of total kinetic energy dissipation. The vertical extent of the domain is from $y^+ \approx 1$ to $y^+ \approx 83$.

Figure 7 b) is again the same sub-volume, this time showing isocontours of total kinetic energy dissipation ($\mathbf{S}_{ij}\mathbf{S}_{ij}$). Once again, the high mean shear near the wall makes it difficult to select a value for the isocontours that can be used to study the boundary layer structure and, as a consequence, the figure becomes relatively featureless.

Robinson [17] did an extensive analysis of the kinematics of turbulence using the same numerical simulation data used here. In particular, the role of vortices as a primary turbulent structure was carefully studied. In that work, the author used the pressure field, specifically regions of low pressure, as a means to identify turbulence structure. The rational was that, for a two-dimensional vortex with circular streamlines, and as a consequence of this assumed symmetry in the velocity field, the pressure has to reach a minimum at the vortex center. In the absence of such circular streamlines, the extrema in the pressure field need not occur.

Figure 8: Close up view of near-wall region showing regions of positive discriminant (blue) and isocontours of pressure (red). a) $p/\rho u_\tau^2 \approx -7.5$. b) $p/\rho u_\tau^2 \approx -4.3$. The vertical extent of the domain is from $y^+ \approx 1$ to $y^+ \approx 83$.

Figure 8 shows the spatial association between the regions of positive discriminant (shown in blue), for the same sub-volume used in Fig. 6, and the pressure field (shown in red). For this figure, the blue isocontours of discriminant have been made transparent so that pressure contours

can be superposed. In Fig. 8 a), a particular threshold value was chosen ($p/(\rho u_\tau^2) \approx -7.5$) corresponding to the lowest pressure values in the volume. There is a visible degree of spatial correlation between the two regions, but the pressure level chosen was insufficient to reveal the entire horseshoe structure. As the threshold level is changed to $p/(\rho u_\tau^2) \approx -4.3$ (the same level used by Robinson [17]) in Fig. 8 b), the correspondence between the two fields is still apparent but it is no longer universal. The computation of correlation coefficients between discriminant and pressure, which can be used to quantify this observation, is currently being done.

Figure 9: Close up view of near-wall region showing regions of positive discriminant (blue) and isocontours of instantaneous Reynolds shear stress ($u'v'$). a) Regions of positive discriminant. b) Positive and negative Reynolds shear stress. Magenta contours correspond to $u'v'/u_\tau^2 \approx -47$. Yellow contours are $u'v'/u_\tau^2 \approx 54$.The vertical extent of the domain is from $y^+ \approx 1$ to $y^+ \approx 102$.

Another area of interest is what role, if any, these structures defined by the discriminant of the velocity gradient tensor play in the production of turbulence. Figure 9 a) shows a top view of a different sub-volume of the DNS data field. The new dimensions, in wall units, are 518 in the streamwise direction (x^+), 286 in the spanwise coordinate (z^+) and, in the direction normal to the wall, it extends from $y^+ \approx 1$ to 102 or just outside the edge of the log layer. This sub-volume is located near the middle of Fig. 5, at $x^+ \approx 1000$, $z^+ \approx 500$. Once again, the blue contour encloses a region where the discriminant is positive (focus topology). All the areas that are not colored are of node-saddle-saddle type (either stable or unstable). Another hairpin shaped structure of large scale is clearly visible. On Fig. 9 b), surfaces of constant, instantaneous Reynolds shear stress value are superposed ($u'v'$). In the magenta color, the strongest, negative Reynolds stresses are indicated ($u'v'/u_\tau^2 \approx -47$) while the yellow corresponds to the strongest, positive levels ($u'v'/u_\tau^2 \approx 54$). For this flow, a time-averaged profile of $u'v'/u_\tau^2$ reaches a maximum value of -0.87, so the events shown

in the plot are up to 62 times stronger that this mean value. The spatial association between these "bursts" and the $D = 0$ contour is very clear. It is important to observe however that the actual Reynolds stress generation, while immediately adjacent to the points of focus topology, seems to take place in areas of where the local topology is of node-saddle-saddle and not within the structures themselves. This observation is consistent with the results of Robinson [17].

4 Discussion

The importance of vortices in boundary layer turbulence has been argued for many years now. This, in spite of the fact that there is still considerable disagreement as to what constitutes a vortex. The intuitively clear idea that a vortex is a region where the streamlines spiral around a point may not be useful when such a structure is embedded in a turbulent velocity field. In addition, visual interpretation of three-dimensional streamlines, almost always from direct numerical simulations, is a daunting task which is further complicated by fact that streamlines are not Galilean invariant. Two-dimensional information, like that obtained from single and two-point correlations or from the projection of the velocity field onto a particular plane can be potentially misleading.

Perry and Chong [18] showed the particular dangers in trying to interpret three-dimensional flow patterns using two-dimensional streamline projections. In that study, they took the velocity field associated with a Burgers vortex and constructed a projection of such field onto a plane that intersected the vortex axis. By varying the angle of intersection, the streamline pattern visible on that plane changed smoothly from a stretched vortex (at 90° angle) to a compressed vortex (at 60°) to a saddle point (at 0°). A visual interpretation of streamlines projections can only be safely done when such projections are carried out on the canonical planes defined by the eigenvectors of the velocity gradient tensor.

This danger is particularly present in turbulent flow fields where three-dimensional streamlines are difficult to analyze and it is normally problematic to find the proper plane onto which to project them. Figure 10 shows a spanwise cut through the field presented in Fig. 5 the streamwise location of the cut is a about $x^+ \approx 796$. On this plane, the blue regions are again regions of focus topology and, in yellow, are the areas of node-saddle-saddle topology. The red areas are zones where the discriminant value is very small

Figure 10: Spanwise cut of the flow field showing regions of positive discriminant (blue) as well as instantaneous streamlines projected onto the plane.

and, hence, where numerical errors might make it difficult to ascertain the local topology. Superposed on this plot are two-dimensional projections of the turbulent streamlines (shown by the black lines). Near the wall, where the mean shear is high and closely aligned with the streamwise Cartesian coordinate used in the simulation, one of the eigenvectors of $\mathbf{A}_{ij}$ is also in close alignment with the x^+ coordinate. As a result, the $y^+ - z^+$ plane shown in the figure is close to a canonical plane for this region of the flow and, as a consequence, the streamlines that depict a spiraling fluid motion are also regions of where the local topology is of focus type.

Figure 11: Instantaneous streamline pattern. a) Stationary frame of reference. b) Frame of reference moving at the mean speed of the flow.

Away from the wall however, as the mean shear decreases, the alignment of the principal axis of the velocity gradient tensor with the Cartesian coordinate system used in the projection is not as likely. Figure 10 shows several areas where the streamlines seem to indicate the presence of vortical motion that, nonetheless, have a node-saddle-saddle topology (negative discriminant). One of those areas, outlined by the black square located at about $z^+ \approx 700$, y^+190, is magnified in Fig. 11. For this figure, a small volume of data, centered around the aforementioned outline, was extracted from the full simulation. The dimensions of this volume are $101, 67$ and 55 wall units in the streamwise, spanwise and wall normal directions respectively. Figure 11 a) shows the three-dimensional streamlines, constructed

from the velocity field data, and as seen by a stationary observer. Since the streamwise component of the velocity is much higher than both, the spanwise and wall-normal components, the streamlines look almost like straight lines and yield little information about the details of the flow. Figure 11 b) shows the same volume but, for this case, the streamlines are those that would be seen by an observer moving at the mean speed of the flow. More details than in Fig. 11 a) are apparent but the flow pattern is just as difficult to interpret. Different choices for the coordinate system translation velocity will yield vastly different results.

Whether or not the structures identified by the invariants of the velocity gradient tensor (Q and R) and it's discriminant (D) are vortices is not clear. In some cases they probably satisfy almost any definition of such a structure. In others, it may depend on the particular definition chosen. In the end, it may not be important. The primary objective behind the study of turbulence structure is to condense the large amount of information contained in a turbulent field and extract from it the most dynamically important aspects. The topological classification method used here provides a rigorous way of looking into both the small as well as the large, organized scales of motion in the flow and the results presented suggest that this may be a useful one in addressing such an objective.

5 Conclusions

The invariants of the velocity gradient tensor (Q and R) were used to study the structure of a turbulent boundary layer. The joint probability distribution of these invariants shows many of the same trends that have been observed in other turbulent flows. These trends include the overall tear-drop shape of the distribution as well as a preference for topologies of the type the stable-focus stretching and unstable-node-saddle-saddle. This later type was also shown to correspond with motions having high values of turbulent kinetic energy dissipation. In addition to the invariants, the discriminant of $\mathbf{A}_{ij}$ was used to study the large scale features of the flow. The use of these scalar invariants provides a consistent, unambiguous, coordinate and threshold independent framework for the study of turbulent flows.

Computer flow visualization of points that have focus topology ($D > 0$) showed that they form long, coherent regions of large streamwise extent near the wall as well as a significant number of horseshoe-like structures. The shape of these structures is reminiscent of the hairpin eddies proposed

by Theodorsen [1]. Additional results presented here seem to indicate that these structures are important in the turbulence production mechanism. In particular, regions of high instantaneous values of Reynolds shear stress ($u'v'$) occur at the edges of these eddies defined by the $D = 0$ surfaces.

6 Acknowledgments

This paper is dedicated to Peter Bradshaw on the occasion of his sixtieth birthday and in recognition of his outstanding accomplishments in the field of turbulence research.

The authors also would like to express their gratitude to Dr. P. Spalart. His help and patience in providing and setting up his direct numerical simulation code have been indispensable. This work was supported by NASA Grant NAG-1-1610. Supercomputer resources have been provided by the San Diego Supercomputer Center.

7 Nomenclature

Roman Symbols

$\mathbf{A}_{ij}$	Velocity gradient tensor ($\partial U_i/\partial x_j$)
D	Discriminant of the velocity gradient tensor $\mathbf{A}_{ij}$
$det[\,]$	Determinant of a tensor
P	First invariant of the velocity gradient tensor $\mathbf{A}_{ij}$
p	Instantaneous pressure
Q	Second invariant of the velocity gradient tensor $\mathbf{A}_{ij}$
R	Third invariant of the velocity gradient tensor $\mathbf{A}_{ij}$
Re_θ	Reynolds number based on momentum thickness
$\mathbf{S}_{ij}$	Rate of strain tensor
$tr[\,]$	Trace of a tensor
U_i	Instantaneous velocity component
$u'v'$	Instantaneous Reynolds stress tensor component
u_τ	Wall shear velocity.
x_j	Cartesian coordinate direction
x^+, y^+, z^+	Cartesian coordinate axis normalized by wall units (u_τ and ν) as defined in Fig. 5
$\mathbf{W}_{ij}$	Rate of rotation tensor

Greek Symbols

λ	generic eigenvalue of the velocity gradient tensor
ν	kinematic viscosity
ρ	Fluid density
θ	Boundary layer momentum thickness

References

[1] Theodorsen, T. 1955. "The structure of turbulence". In *50 Jahre Grenzschichtforsung.* Ed. H. Görtler, W. Tollmein. pp. 55 - 62.

[2] Perry, A. E., Marušić. I. and Li, J. D. 1994. "Wall turbulence closure based on classical similarity laws and the attached eddy hypothesis". *Applied Scientific Research.* **6** (2). pp. 1024 - 1035.

[3] Townsend, A. A. 1956. "The structure of turbulent shear flow". Cambridge Univ. Press. 1^st ed.

[4] Blackburn, H. M., Mansour, N. N. and Cantwell, B. J. 1996. "Topology of fine-scale motions in turbulent channel flow". *J. Fluid Mech.* **310**. pp. 269 - 292.

[5] Taylor, E. S. 1967. "Some problems of recognizing and defining separation of the skewed boundary layer". In *Fluid Mechanics of Internal Flow.* pp. 320 - 332. Elsevier, Amsterdam.

[6] Oswatitsch, K. 1958. "Die Ablösungsbedingung von Grenzschichten". *Grenzschichtforschung.* Berlin/Göttingen/Heidelberg.

[7] Perry, A. E. and Fairlie, B. D. 1974. "Critical points in flow patterns". *Adv. Geophysics* **18B**. pp. 299 - 315.

[8] Chong, M. S., Perry, A. E. and Cantwell, B. J. 1990. "A general classification of three-dimensional flow fields". *Phys. Fluids A* **2** (5). pp. 765 - 777.

[9] Chen, J. H., Chong, M. S., Soria, J., Sondergaard, R., Perry, A. E., Rogers, M., Moser, R. and Cantwell, B. J. 1990. "A study of the topology of dissipating motions in direct numerical simulations of time-developing compressible and incompressible mixing layers". *Proceedings*

of the Summer Program. Center for Turbulence Research. Stanford University. pp. 139 - 161.

[10] Soria, J. and Cantwell, B. J. 1994. "Topological visualization of focal structures in free shear flows". *Applied Scientific Research.* **53.** (3-4) pp. 375 - 386.

[11] Soria, J., Sondergaard, R., Cantwell, B. J., Chong, M. S. and Perry, A. E. 1994. "A study of the fine-scale motions of incompressible time-developing mixing layers". *Phys. Fluids* **6** (2) Pt. 2. pp. 871 - 884.

[12] Boratav, O.N. and Pelz, R. B. 1995. "On the local topology evolution of a high-symmetry flow". *Phys. Fluids* **7** (7). pp. 1712 - 1731.

[13] Kim, J., Moin, P. and Moser, R. 1987. "Turbulence statistics in fully developed channel flow at low Reynolds number". *J. Fluid Mech.* **177.** pp. 133 - 166.

[14] Spalart, P. R. 1988. "Direct simulation of a turbulent boundary layer up to $Re_\theta = 1410$". *J. Fluid Mech.* **187.** pp. 61 - 98.

[15] Perry, A. E. and Chong, M. S. 1987. "A description of eddying flow patterns using critical-point concepts". *Ann. Rev. Fluid Mech.* pp. 125 - 155.

[16] Head, M. R. and Bandyopadhyay, P. 1978. "Combined flow visualization and hot wire measurements in turbulent boundary layers". In *Lehigh Workshop on Coherent Structure in Turbulent Boundary layers.* Ed. C. R. Smith. pp. 98 - 125.

[17] Robinson, S. K. 1991. "Coherent motions in the turbulent boundary layer". *Ann. Rev. Fluid Mech.* pp. 601 - 639.

[18] Perry, A. E. and Chong, M. S. 1994. "Topology of flow patterns in vortex motions and turbulence". *Applied Scientific Research.* **53.** pp. 357 - 374.

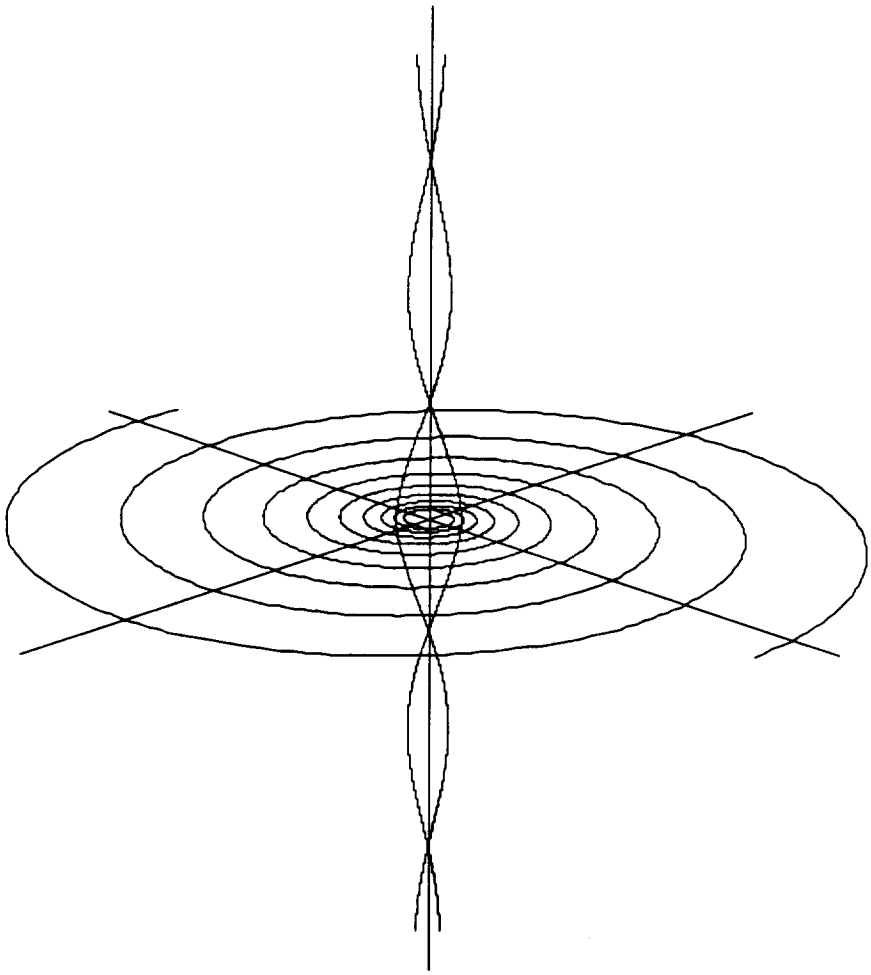

Figure 1: Idealized streamline pattern around a focus critical point.

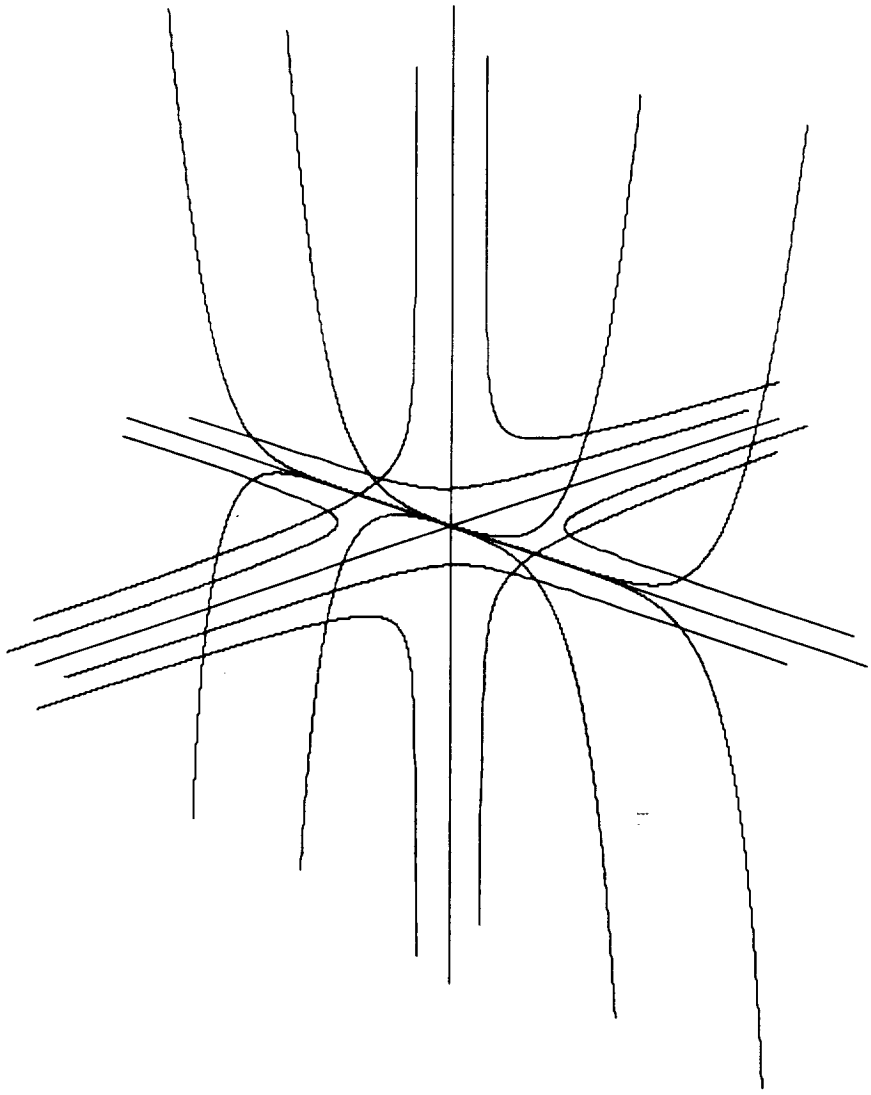

Figure 2: Idealized streamline pattern around a node-saddle-saddle critical point.

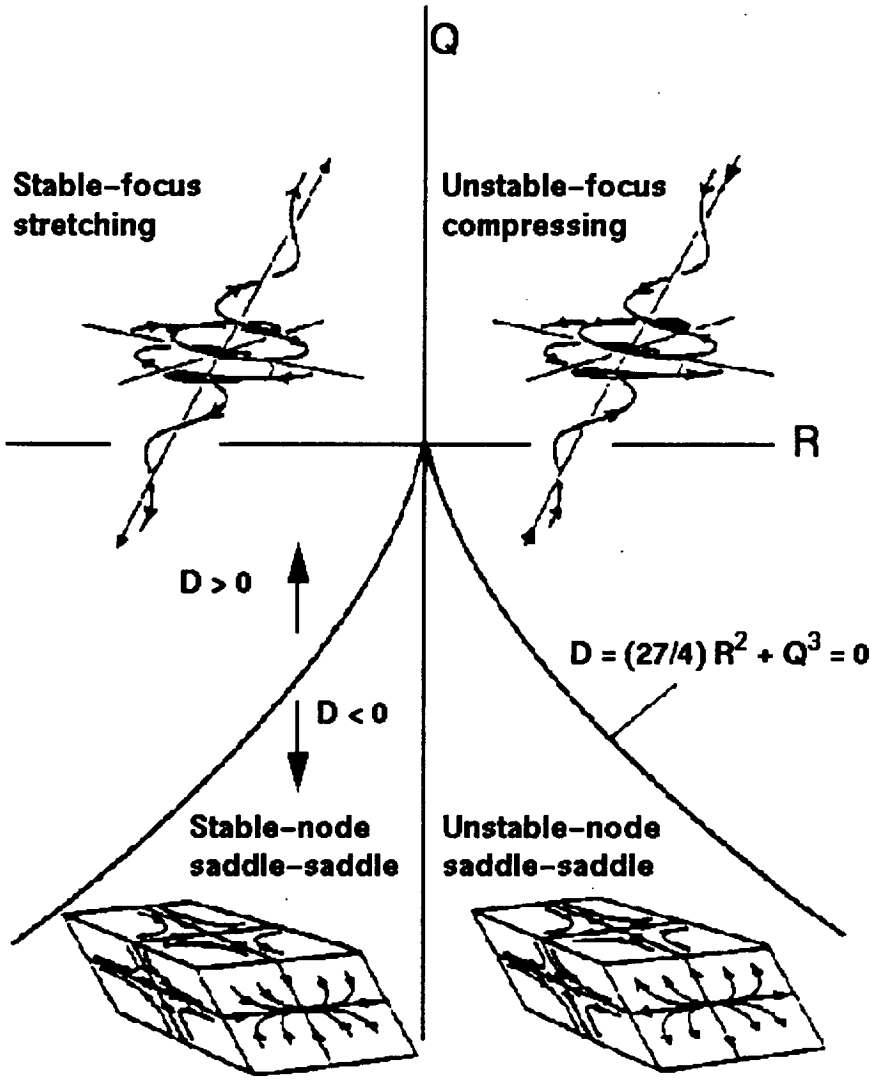

Figure 3: Summary of three dimensional incompressible topologies (from Soria *et. al.* [11]).

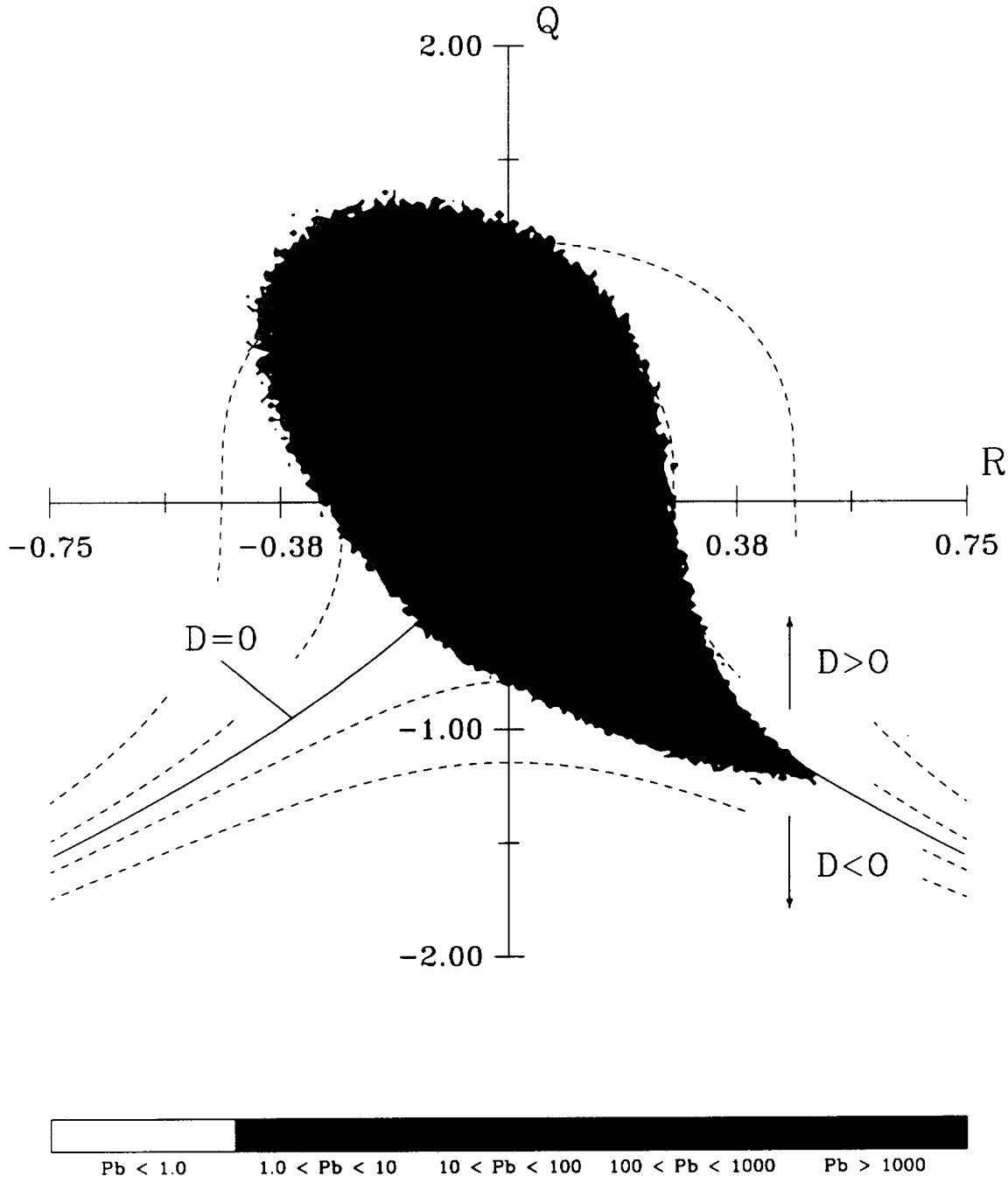

Figure 4: Time-averaged, unnormalized joint probability density distributions for the second and third invariants of the velocity gradient tensor (Q and R). The dashed lines are lines of constant discriminant (Eq. 7). The values grow or decrease as indicated by the arrows.

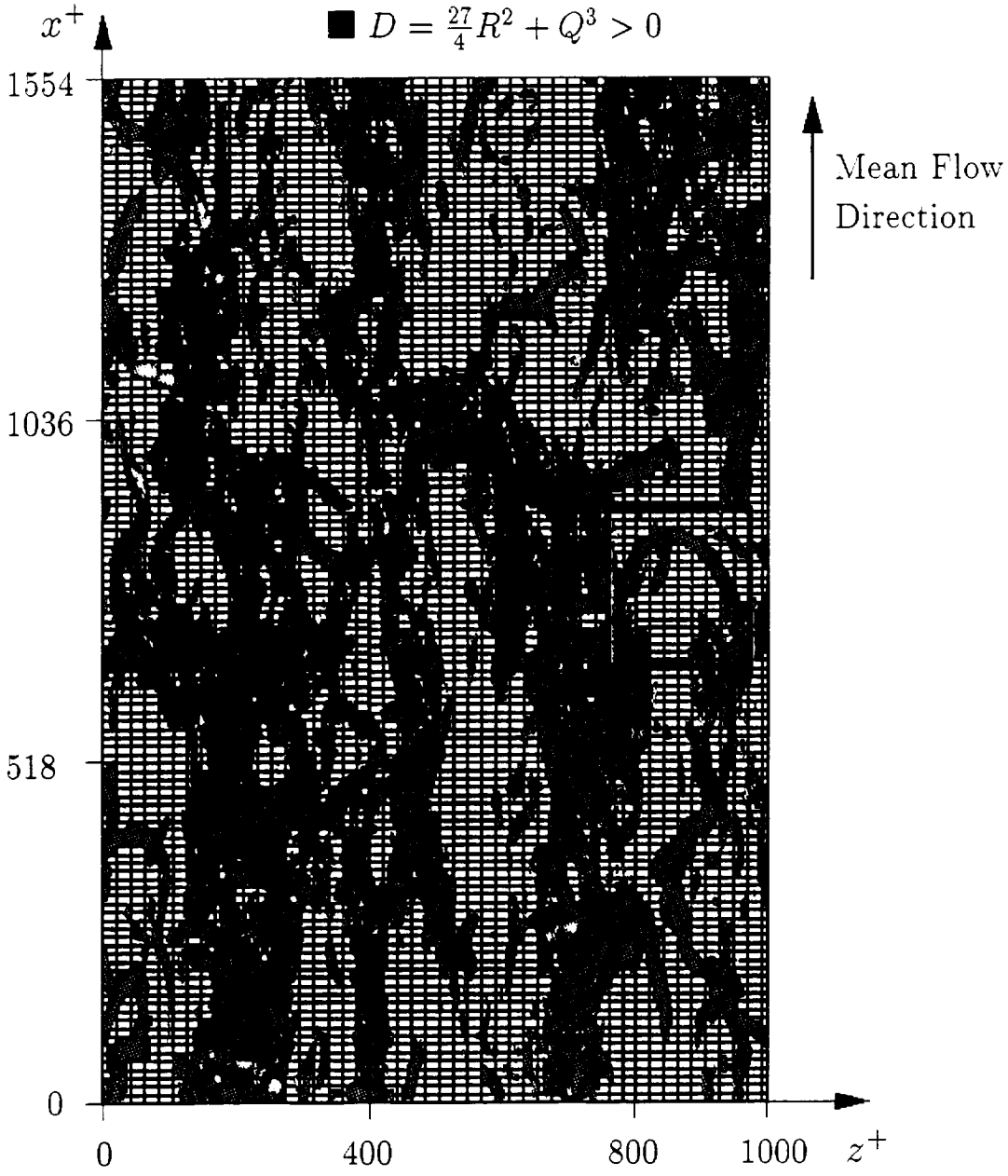

Figure 5: Top view of the computational volume. The blue contours are regions of positive discriminant (focus topology). The vertical extent of the domain is from $y^+ \approx 1$ to $y^+ \approx 138$. All the areas that are not colored have topology of the type node-saddle-saddle.

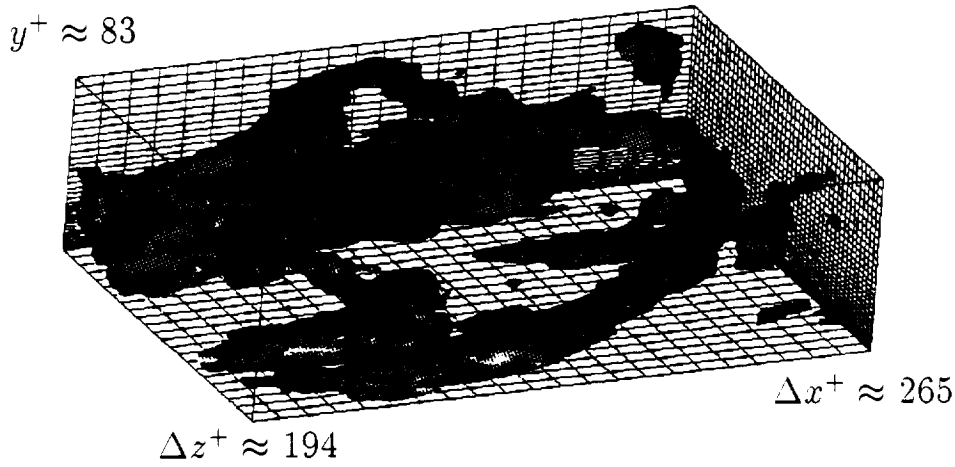

a)

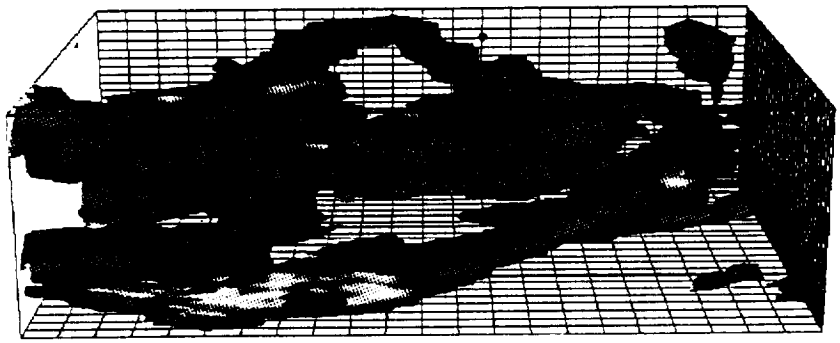

b)

Figure 6: a) Close up view of a near-wall region of positive discriminant. b) Side view of the same region. The vertical extent of the domain is from $y^+ \approx 1$ to $y^+ \approx 83$.

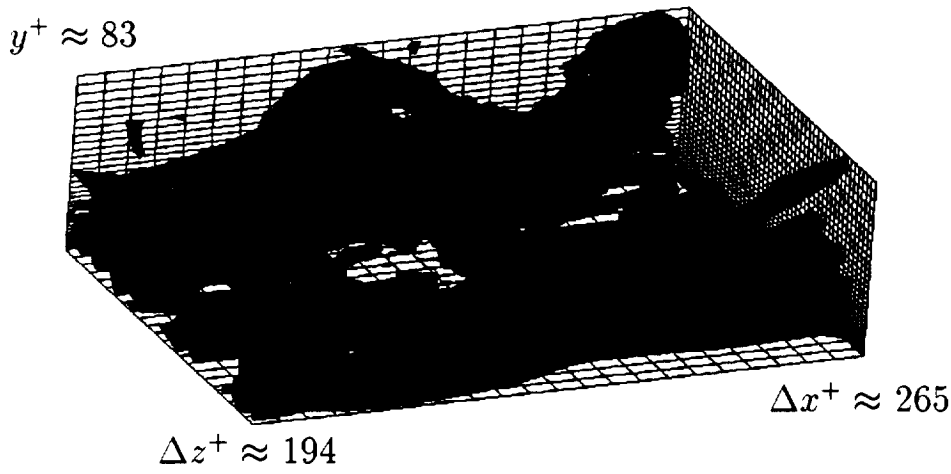

a)

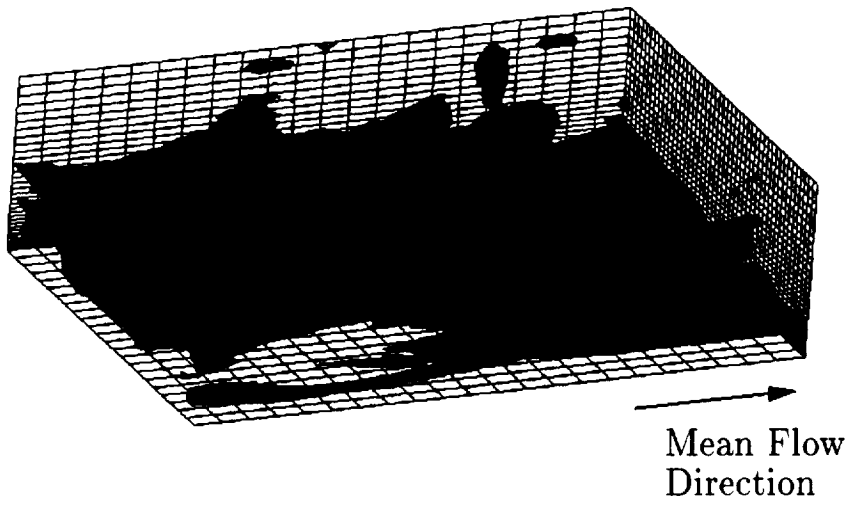

b)

Figure 7: Close up view of near-wall region. a) Isocontours of total vorticity magnitude. b) Isocontours of total kinetic energy dissipation. The vertical extent of the domain is from $y^+ \approx 1$ to $y^+ \approx 83$.

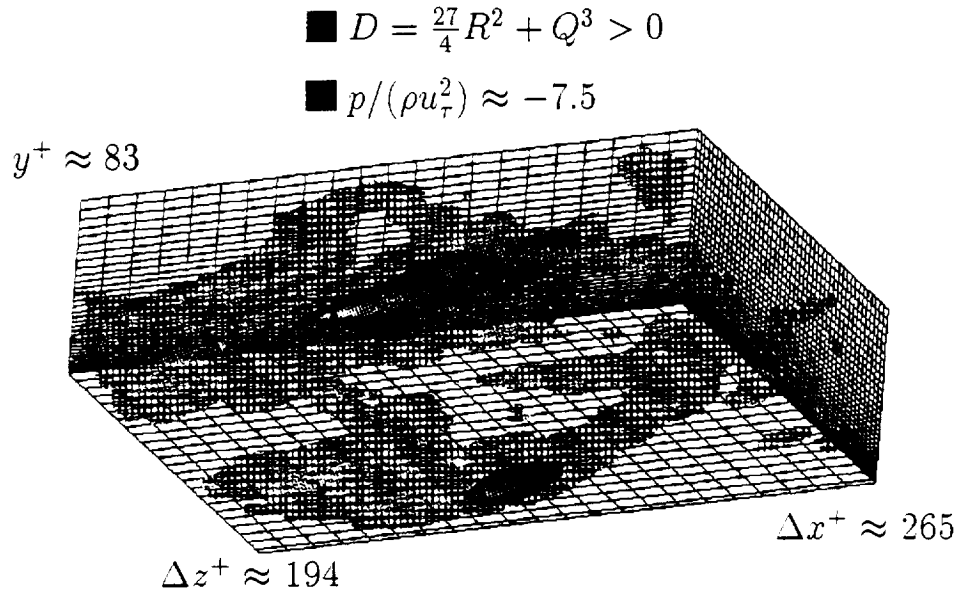

a)

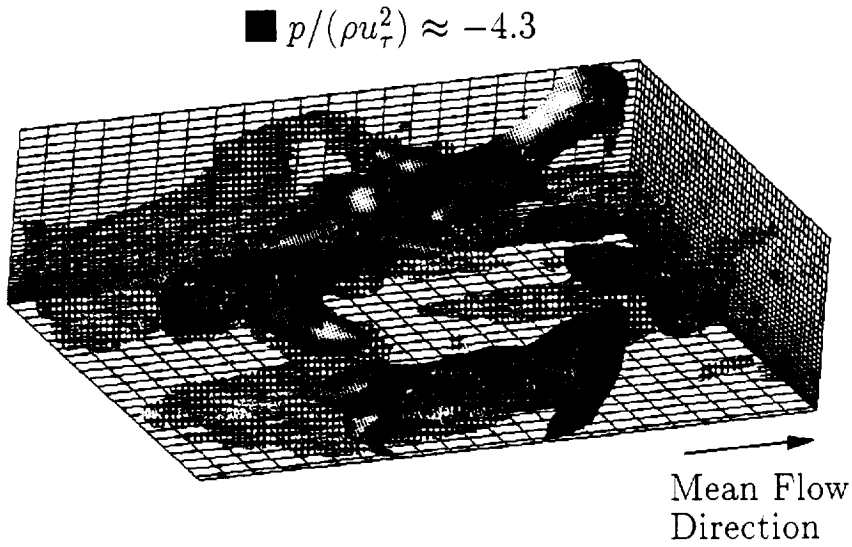

b)

Figure 8: Close up view of near-wall region showing regions of positive discriminant (blue) and isocontours of pressure (red). a) $p/\rho u_\tau^2 \approx -7.5$. b) $p/\rho u_\tau^2 \approx -4.3$. The vertical extent of the domain is from $y^+ \approx 1$ to $y^+ \approx 83$.

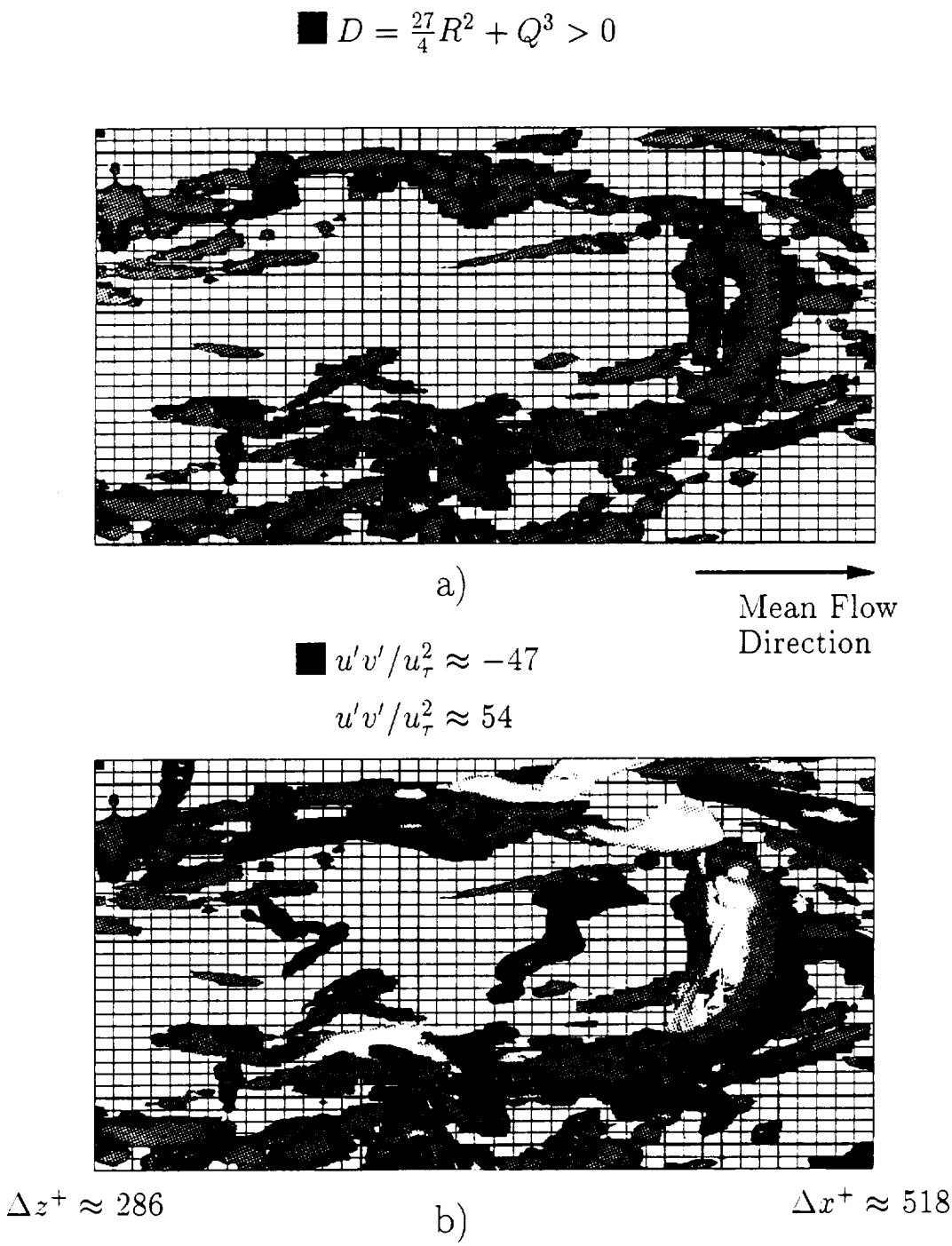

Figure 9: Close up view of near-wall region showing regions of positive discriminant (blue) and isocontours of instantaneous Reynolds shear stress ($u'v'$). a) Regions of positive discriminant. b) Positive and negative Reynolds shear stress. Magenta contours correspond to $u'v'/u_\tau^2 \approx -47$. Yellow contours are $u'v'/u_\tau^2 \approx 54$.The vertical extent of the domain is from $y^+ \approx 1$ to $y^+ \approx 102$.

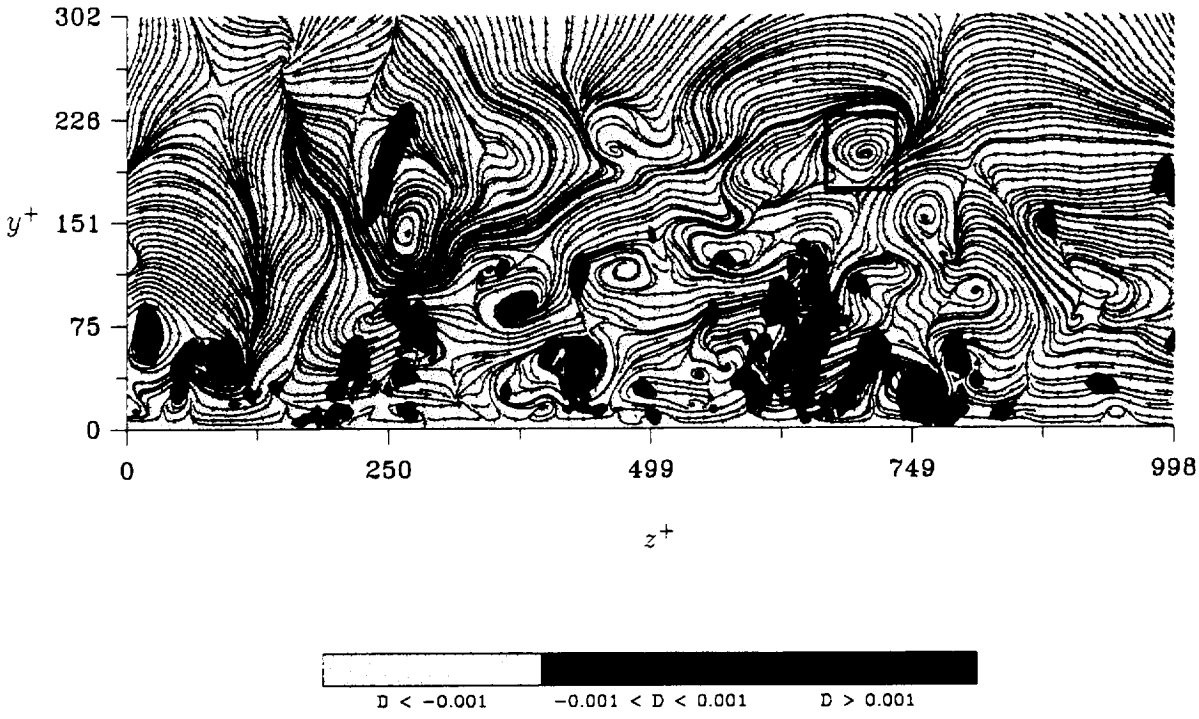

Figure 10: Spanwise cut of the flow field showing regions of positive discriminant (blue) as well as instantaneous streamlines projected onto the plane.

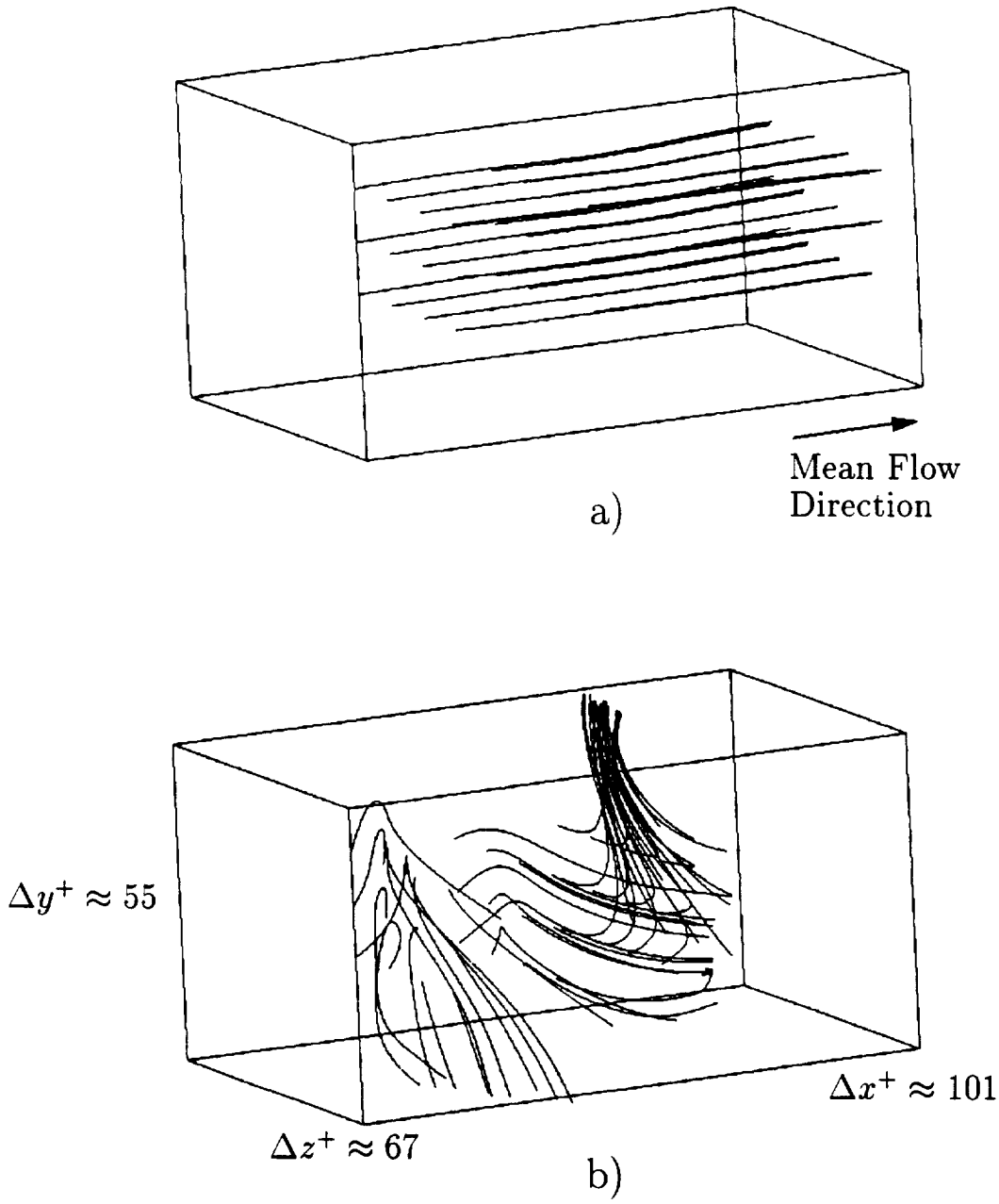

Figure 11: Instantaneous streamline pattern. a) Stationary frame of reference. b) Frame of reference moving at the mean speed of the flow.